Observations on the location, mechanisms and consequences of impurity generation with a poloidal divertor in DIII-D

D.G. Whyte,*University of California, San Diego, 92093-0417 USA*
e-mail address: dwhyte@ucsd.edu

1. Introduction

One of the primary motivations in using a poloidal divertor is the control of impurities. The divertor magnetic configuration successfully moves the intense locations of heat and recycling far away from the immediate periphery of the core plasma. Indeed, the use of divertors has generally lead to improved operation flexibility, especially in regard to tolerance of over-heating events at plasma-facing surfaces. Nevertheless, the use of poloidal divertors in current devices has not necessarily resulted in obvious control of impurities in the core plasma[1].

Unlike current confinement experiments*, future burning plasmas must have control over the generation and consequences of impurities in the plasma*. Fuel dilution and Z_{eff} of the core plasma must be below critical values in order to obtain ignition. The erosion/redeposition (E/R) associated with the sputtering and transport of impurities will limit wall viability. Tritium fuel trapping in deposits is also a significant safety and economic concern.So a vital question remains to be answered: **what is the location, and cause, of the material sputtering that gives rise to the core plasma impurity content in diverted plasmas?** The answer to this question speaks directly to core contamination issues. It also touches on the related issues of E/R and fuel trapping, since the impurities that find their way to the core plasma undergo poloidal redistribution after re-entering the SOL. Unlike eroded material that is promptly redeposited locally, the core impurities lose the "memory" of their initial location and are subject to the global edge transport patterns that determine E/R.

2. Empirical study of impurity sources on DIII-D

Empirical methods are used to answer the question of core impurity sources on the DIII-D tokamak operating with single-null divertor magnetic geometry. From physics-based ideas of SOL transport and erosion, we perform experimental tests to affect core impurity levels. This is contrasted to the common approach of relying on edge modeling codes to examine impurity issues. The advantage of the empirical approach is that by definition we include all the parameters of the edge plasma and wall that are difficult to diagnose and include in modeling codes. The drawback of the empirical approach is that is difficult to uncover a definitive "independent" experimental variable to affect impurities. Clear parametric scans concerning particle sources and sinks are nearly impossible in edge plasma experiments because the system variables are strongly couple, usually in a non-linear fashion.

Four experimental methods are use to vary the relationship between fuel recycling, impurity sputtering and the fuel/impurity transport**.**

1. The geometry of the plasma and wall surfaces is varied. This exploits the expectation that fuel and impurities penetrate and transport through the edge plasma with different scale-lengths.
2. The modification of wall material erosion properties by changes of the wall material composition.
3. The modification of edge plasma properties, especially in regard to its sputtering capacity.
4. The enhanced removal/erosion of wall materials by thermal processes such as melting or sublimation.

In this paper we compile empirical evidence on impurity source locations in DIII-D, specifically examining the relative role of divertor targets versus the main-wall. The comprehensive edge plasma and impurity diagnostics of DIII-D are used [2]as well as the flexible plasma shaping control in the relatively open lower divertor. Carbon is the only

impurity considered: it is the dominant impurity in DIII-D owing to the all-graphite coverage of the walls. The core carbon fraction ($f_{carbon} = n_{carbon}/n_e$) is measured accurately by charge-exchange spectroscopy of fully ionized carbon[3].

2.1 Divertor sources do not correlate to the core impurity level

The absence of an obvious correlation between divertor target impurity sources and the core plasma impurity level has been noted on several tokamaks [1]. This observation is confirmed and expanded upon in DIII-D by using the four experimental techniques described above.

Divertor geometry does not strongly affect f_{carbon}. A large scan of the divertor length with an X-point height scan (**Fig. 1**) shows no reduction in f_{carbon} as the divertor leg is extended to its practical limit[4]. Neither is there any significant change in the conducted power fraction to the divertor targets with increasing divertor leg length. The core impurity level is somewhat higher when the plasma is essentially limited at very small X-point heights. A variation of the divertor "openness" using a strikepoint scan in the lower divertor (**Fig. 2**) also shows no trend in f_{carbon}.

Boron has become an integral part of the DIII-D graphite over the last decade due to over 40 boronizations on the same tiles in the lower divertor. Boron-doping has reduced the chemical erosion yield, Y_{chem}, of the low divertor targets (**Fig. 3**)[5]. The reduction in Y_{chem} has resulted in a considerable overall reduction in the total carbon source from the lower divertor target, yet no appreciable reduction has occurred in the core plasma carbon fraction for the ELMy H-mode discharges used in the erosion database (**Fig. 3**).
The elimination of physical sputtering at divertor targets via detachment does not affect core impurity level (**Fig. 4**). Physical sputtering of carbon by deuterium has a threshold energy $\sim$ 25 eV. Therefore, when the plasma T_e falls below 5 eV ($E_i\sim 5\ T_e$ from sheath theory), the divertor target plasma can no longer sustain physical sputtering. For $T_e > 10$ eV, physical sputtering accounts for more than half of the effective carbon removal in the divertor, yet its elimination has no affect on f_{carbon}.
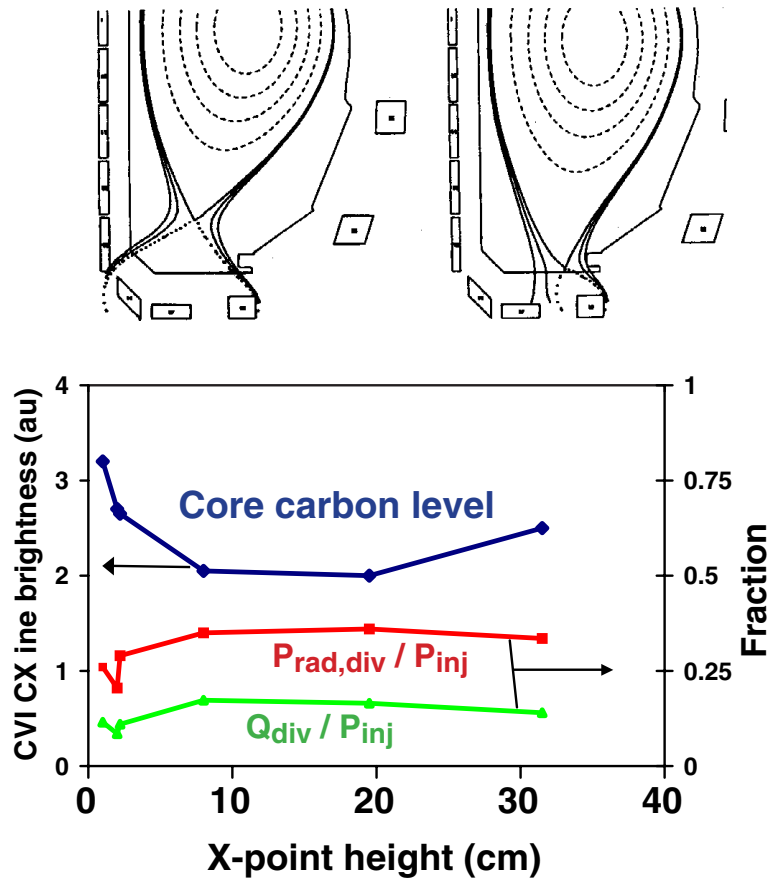
Fig. 1
(Top) X-point height scan in ELMy H-mode plasmas with injected power P=6.8 MW.
(Bottom) Core carbon fraction (f_{carbon}) and divertor radiated/conducted power fractions
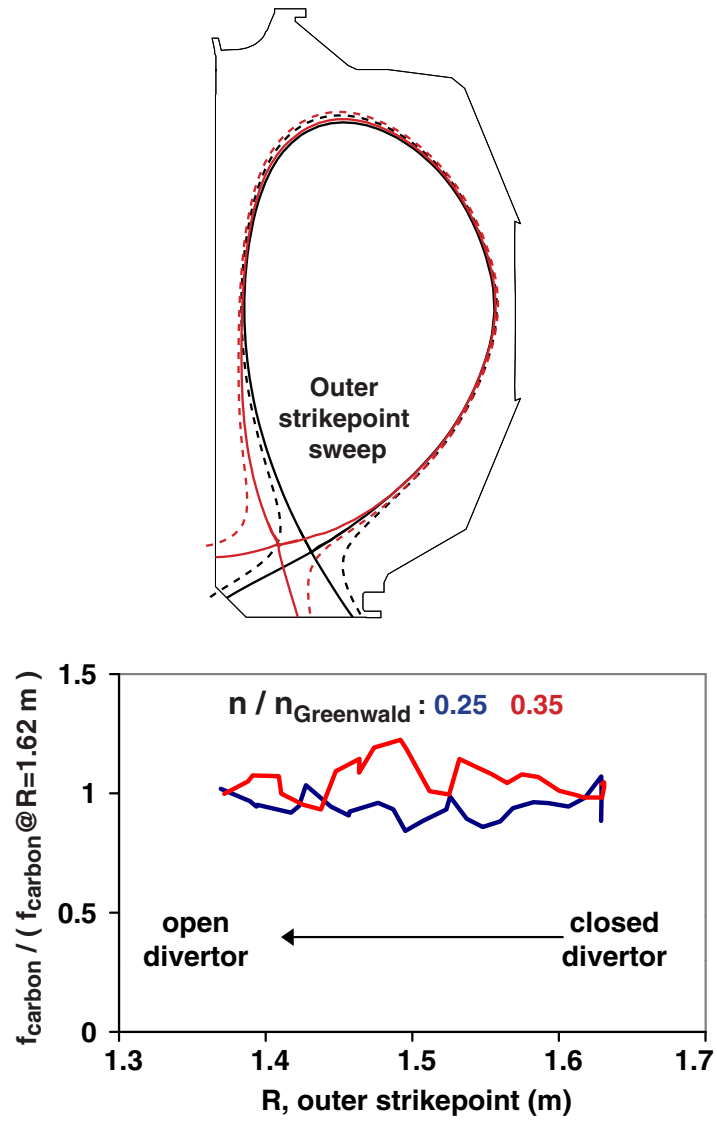vs. X-point height.

Fig. 2
(Top) Divertor outer strikepoint (OSP) radial sweep with L-mode plasmas (P~1.8 MW).
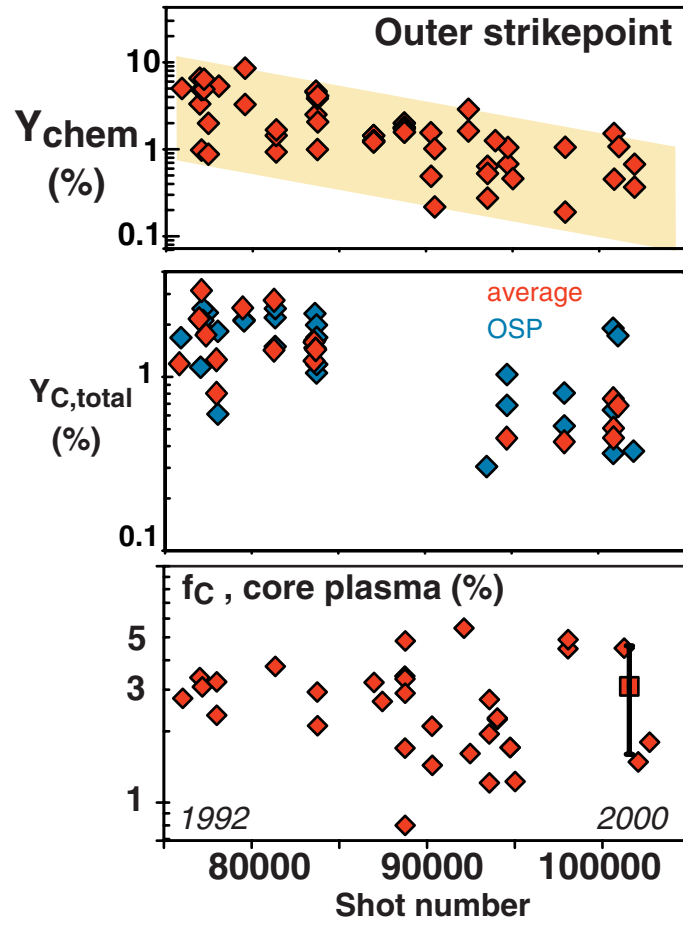(Bottom) Core carbon fraction, f_{carbon} vs. OSP radius at two densities.

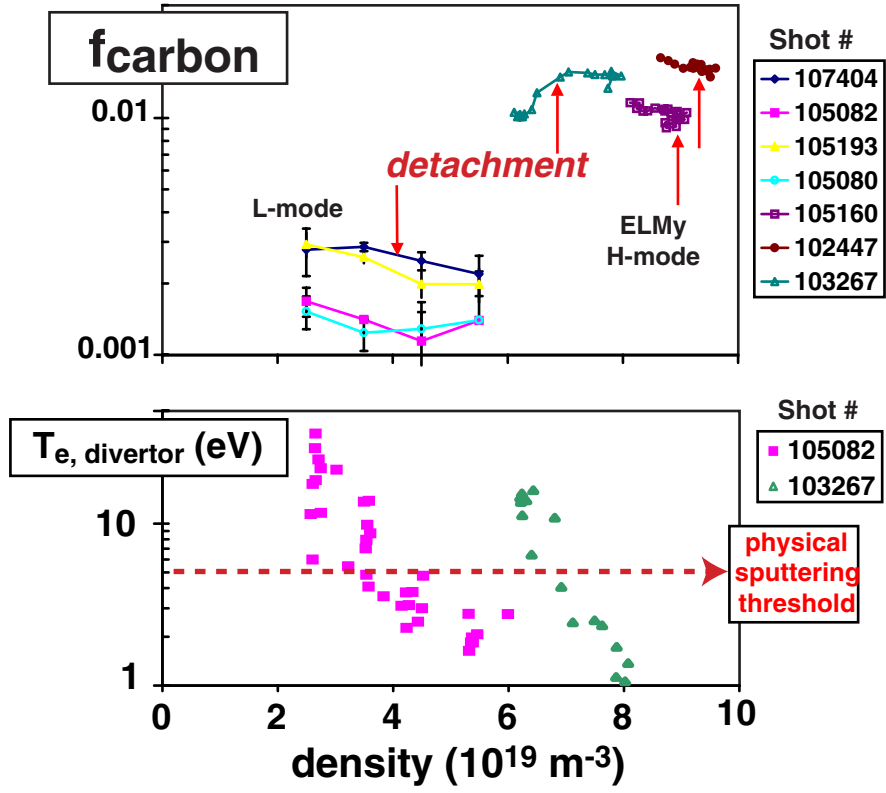**Fig. 4**

Core carbon fraction, f_{carbon} and divertor target electron temperature, $T_{e,div}$ versus line-averaged density for L-mode and H-mode plasmas. Arrows indicate point of outer divertor leg detachment in each scan: $T_{e,div}$ falls below 5 eV and physical sputtering is eliminated.

Increasing the divertor target carbon erosion through heating does not increase the core impurity level. Local carbon spectroscopy and infrared imaging confirm the presence of tile edge sublimation at both the outer and inner strikepoint of beam-heated discharges. Sublimation leads to local enhancements of approximately a hundredfold in carbon removal rate (**Fig. 5**). However, the intentional sublimation of a leading edge lip (inserted on the DiMES probe) does not increase f_{carbon} compared to operating on flat tile surfaces. Similarly, alternating the upper inner strikepoint between inner-wall regions with contoured and faceted tiles significantly affects tile sublimation (**Fig. 6**), with temperatures > 2500 K measured at faceted tile edges. While the tile sublimation increased the local carbon ion source rate from the inner divertor, it has no effect on f_{carbon}. Likewise the continued heating of tiles and tile edges for more than four seconds does not result in an increasing f_{carbon} during the discharge.

Chemical erosion also has a temperature dependence, with Y_{chem} peaking at $T_{max} \sim 600$ K. Since DIII-D operates the wall with a baseline temperature ~ 300-350 K, we expect the divertor target region to move through this peak within a single beam-heated discharge (see temperature calculations for **Fig. 5**). Apparently then, divertor target chemical erosion also has no effect on f_{carbon} from either the inner or outer divertor.

Based on the empirical evidence we conclude that the divertor shields the core plasma very well from thermally removed carbon. This is clearly a desirable trait, especially with regard to managing the over-heating of divertor target surfaces.

We note that Guo et al. [6] showed a correlation of increasing carbon sources and f_{carbon} with increasing baseline wall temperature (to $\sim T_{max}$) on JET. However, the location of the controlling chemical erosion was uncertain since both the divertor and main-wall baseline temperatures were changed together. Combining the JET result with the DIII-D result of no f_{carbon} correlation to divertor target heating through T_{max}, we might conclude that the main-wall is the controlling location for chemical erosion. Indeed this is in agreement with the DIII-D empirical evidence examined in the next section.
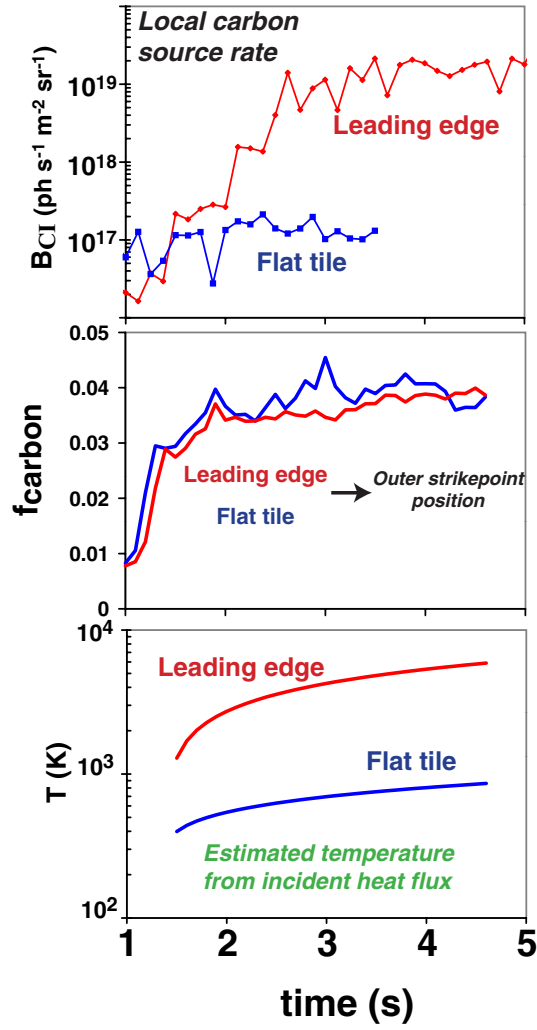
Fig. 5
Time traces of local divertor source (from outer strikepoint CI emission), core carbon fraction and calculated tile temperatures for lower single-null discharges with P~12 MW. Discharges have fixed outer strikepoint positioned either on a flat tile or on a graphite 0.7 mm leading edge lip on the DiMES probe.
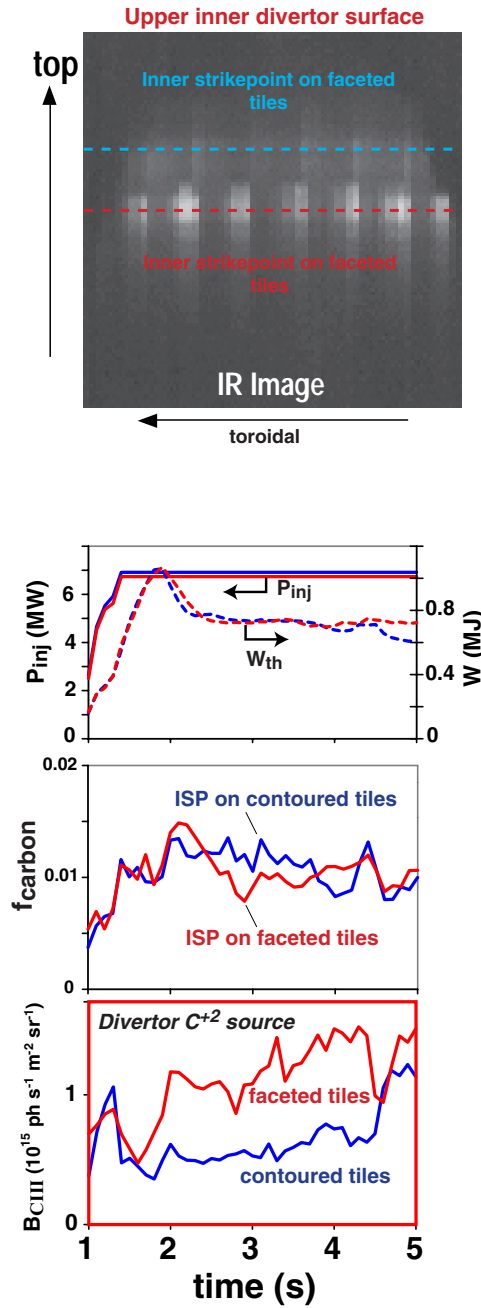
Fig. 6
(Top) Infrared image of upper inner divertor tile surfaces compares toroidally non-uniform heating of faceted centerpost tile edges versus approximately uniform heating of contoured tiles. (Bottom panels) Time traces of injected power, P_{inj}, core plasma thermal energy, W_{th}, carbon fraction, f_{carbon} and inner divertor target C^{+2} source for comparison discharges with the inner strikepoint positioned on contoured or faceted inner wall sections.

2.2 Main-wall sources do correlate to the core impurity level

Geometry and material effects are assessed with regard to the correlation of main-wall carbon erosion and f_{carbon}. We note that detachment and sublimation (i.e. methods 3-4 listed above) are not available to vary the main-wall erosion.

In contrast to the divertor, main-wall carbon erosion yield has not been altered by the history of boronizations, consistent with the approximately constant core impurity level (**Fig. 7**)[7]. The constant main-wall carbon erosion yield is consistent with the fact that boron doping only affects chemical erosion in divertor target regions with T > 400 K. Unfortunately the uncontrolled core plasma parameters in the H-mode erosion database leads to significant scatter in f_{carbon} and midplane carbon source. However, an additional database consisting of very similar L-mode discharges (used for L-H power threshold studies) shows a consistent correlation of midplane CIII and f_{carbon}. We speculate that the variations in midplane carbon source yield in the L-mode database are due to the partial covering of main-wall graphite surfaces with boron[8]. Since boron coverage evolves after the application of each boronization, one expects some random variation in the database depending on immediacy to boronizations and exposure history.

Geometry/ gap changes are the most powerful tool for main-wall surface impurity studies. Simply stated, as the gap between the last-close flux surface (LCFS) and the wall is reduced, we expect better access for the eroded carbon to enter the core plasma. Core parameters (P_{inj}, W_{th}, n_e, etc.) can be kept constant during gap scans, making them ideal for studying f_{carbon} correlations. On DIII-D lower single-null discharges we vary the gap between the LCFS and two main-wall surfaces: the outer midplane and the knee of the upper divertor baffle (**Fig. 8**). The outer midplane has the advantage of radially resolved local deuterium and carbon visible spectroscopy and a survey XUV spectrometer; however the non-axisymmetry of the outer midplane limiting surfaces makes interpretation more difficult. The upper baffle knee is an axisymmetric surface and is instrumented with a Langmuir probe, however it lacks spatially resolved spectroscopy diagnostic coverage.
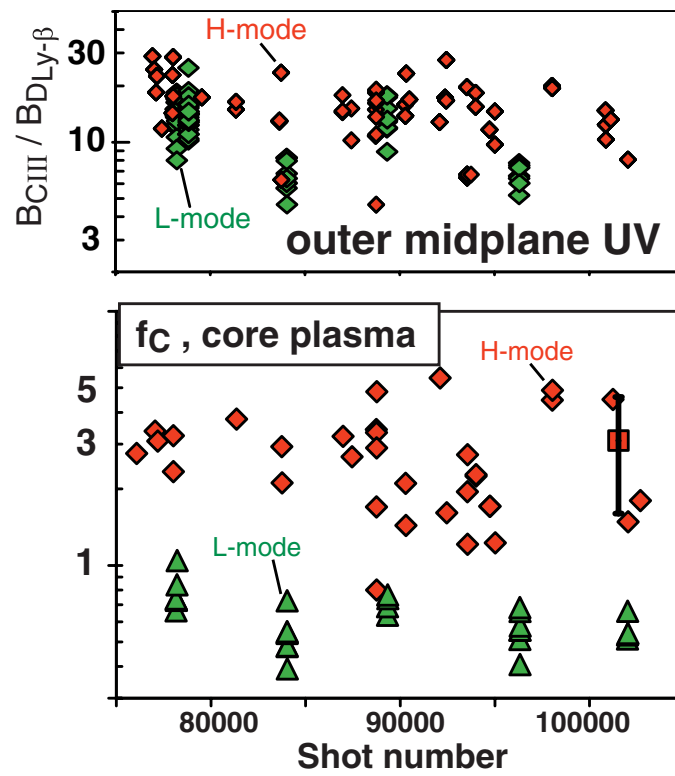
Fig. 7
(Top) Historical trend of measured midplane C^{+2} source yield using XUV spectrometer in both L-mode and H-mode. (Bottom) Same for core carbon fraction.

Fig. 8
Schematics of geometry/gap scans and relevant diagnostics used for main-wall impurity studies. (Left) Gap scans of last-closed flux surface (LCFS) to non-axisymmetric outer midplane (insert). (Right) Gap scans of LCFS to axisymmetric upper baffle knee.

Core impurity level correlates well to the gap between LCFS and the outer midplane limiter surface in several confinement regimes studied: L-mode, ELMy H-mode and ELM-free H-mode (**Fig. 9**).outer midplane impurity influx and recycling increase as expected from increasing plasma contact with the closing gap (i.e. the limiter is moved further into the SOL plasma). We note that "well-diverted "cases (i.e. the largest LCFS-wall gaps) have the lowest core impurity level while the near-limited cases have the highest.

Similarly, f_{carbon} and local carbon source correlates well to the LCFS gap distance to the axisymmetric upper baffle knee (**Fig. 10**). The main-wall impurity source to f_{carbon} correlation is robust over wide range of densities and through divertor detachment. The trends in local carbon erosion flux at the knee are consistent with plasma flux measured with the Langmuir probe at the baffle knee limiter surface. Again, the near-limited case has the highest impurity level.

It is also informative to examine the reaction of other poloidal locations to the local gap scan (**Fig. 11**). Global recycling/refueling is not conserved during the gap scan, with the gas fuelling rate decreasing sharply as the plasma becomes marginally limited. This is understood from the idea that better fuel penetration is expected from the limiting surface and less total recycling is needed to sustain a given core density. However, since impurities are not constrained in satisfying the constant density condition, we expect and find better impurity "penetration" for the cases where the limiting surfaces are closer to the LCFS. We also note that as the gap is reduced, f_{carbon} increases before any significant change occurs in recycling and impurity sources at the midplane and outer divertor. The divertor only starts to "turn-off" in the near-limited case, when the heat conduction through the narrow region near the LCFS starts to become blocked by the limiter surface. Finally it is important to note that the recycle and impurity flux of non-limiter poloidal locations is only reduced a factor of 2-3 as the plasma becomes near-limited on the upper baffle knee. This implies that sufficient cross-field transport exists to compete against that parallel particle losses to the limiter.

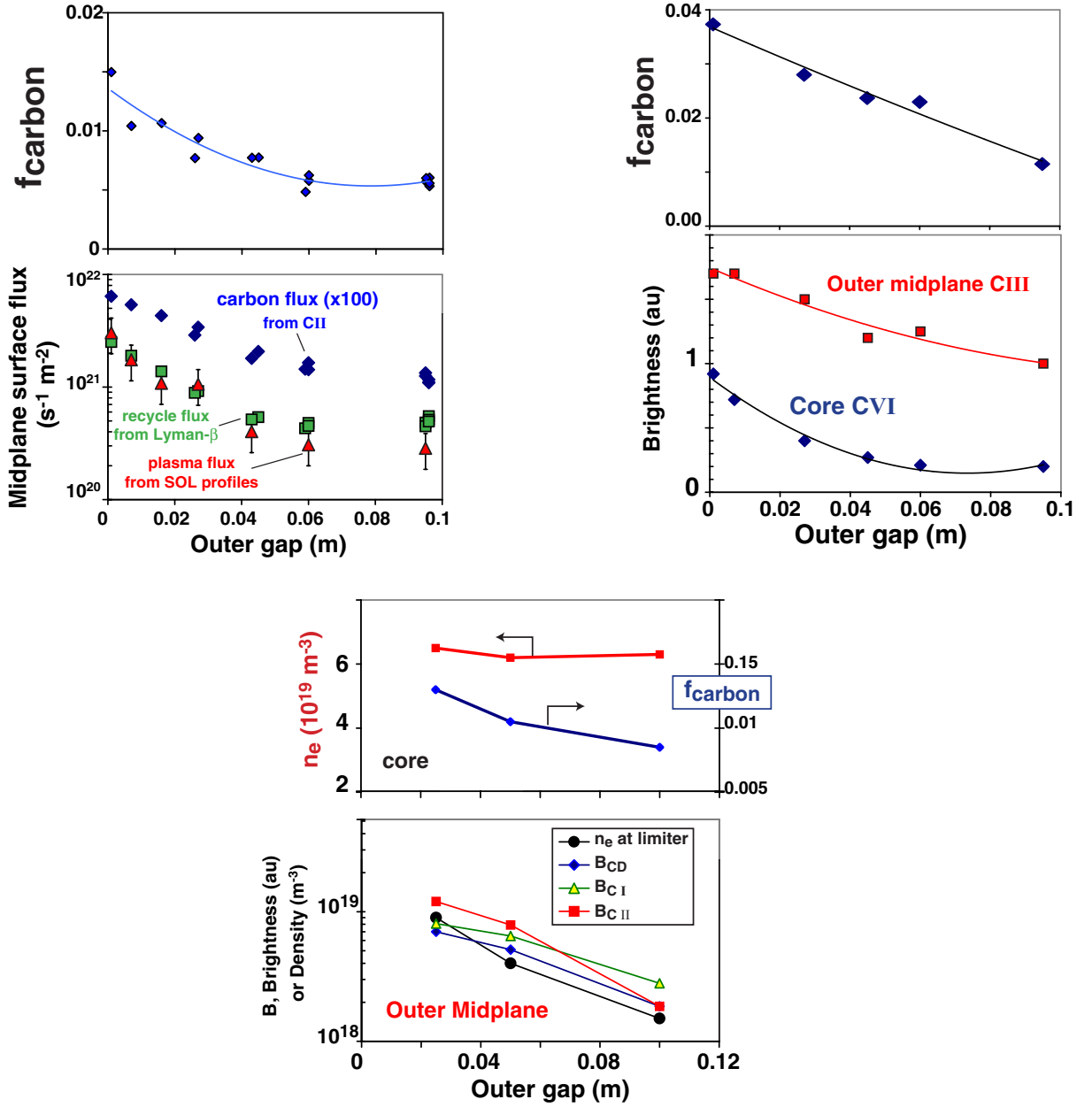**3. On the magnitude and cause of main-wall erosion**

Fig. 9
Results of outer gap scans on core carbon fraction in
(Top left) L-mode: P~1.8 MW, n_e= 4x10^{19} m^{-3},
(Bottom middle) ELMy H-mode: P~7 MW, n_e= 6.5x10^{19} m^{-3},
(Top right) ELM-free H-mode: P > 2MW, n_e= 7.5x10^{19} m^{-3}
Outer midplane plasma flux estimated from SOL profiles measured by Thomson scattering. Outer midplane carbon influx measured from local XUV and visible emission spectroscopy.
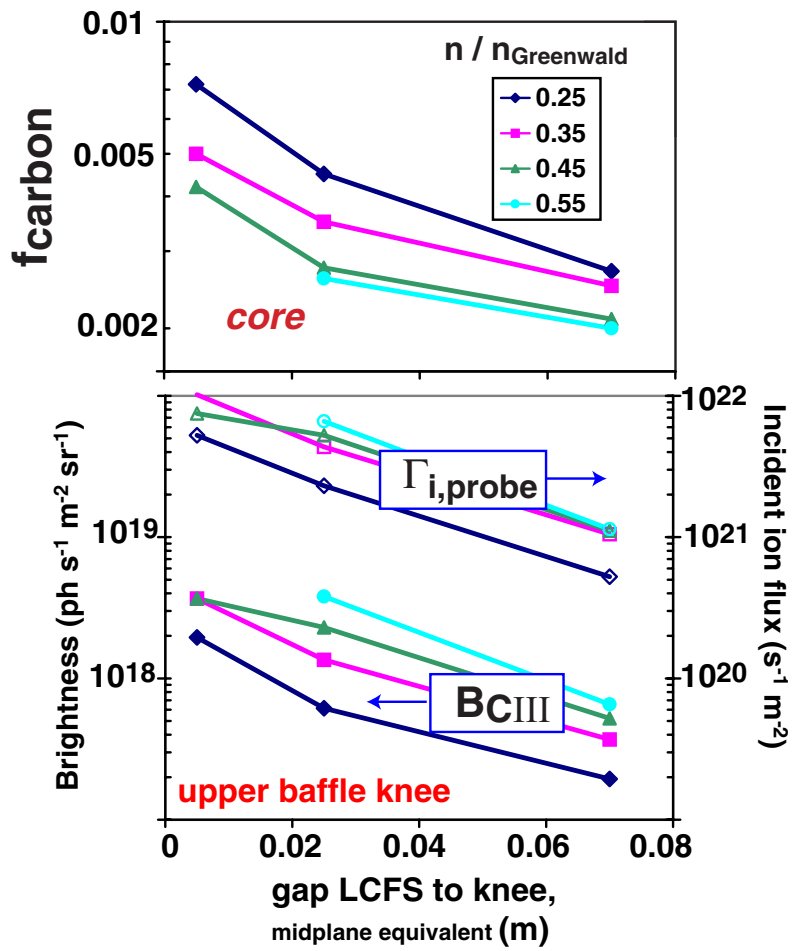
Fig. 10
Results of upper baffle knee gap scans on (top) core carbon fraction (bottom) plasma flux (measured with a probe) and C^{+2} source at the baffle knee/limiter. Gap shown is midplane equivalent flux surface distance.
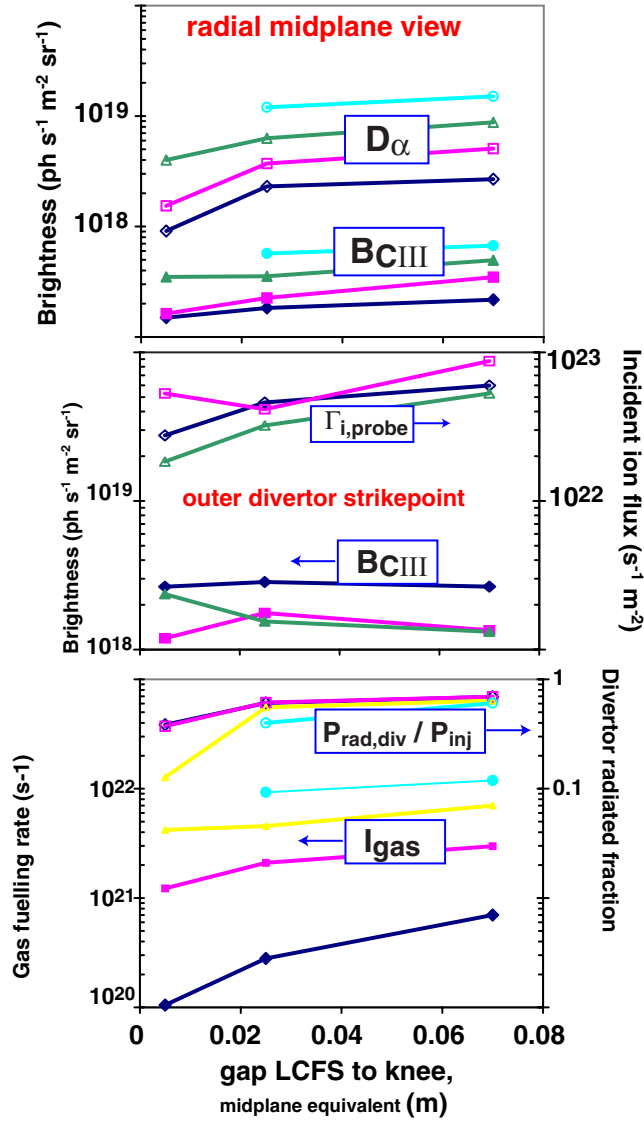
The preceding section demonstrated a clear correlation between LCFS-main wall gaps and f_{carbon}. We also found a consistent lack of correlation between divertor target erosion and f_{carbon}. While this clearly points the finger at the main-wall as the culprit in core impurity sources, it is desirable to ascertain if the absolute magnitude of main-wall erosion sources is sufficient to account for the measured f_{carbon}. Two methods are used to assess magnitude of main-wall impurity sources as related to core impurity level

The first method uses the concept of penetration factor for the carbon impurity. Carbon, in the form of methane gas, is injected at a known rate (I_{carbon}) from the main-wall. The measured change in core impurity inventory, ΔN_{carbon}, establishes the penetration factor, PF [s] = $\Delta N_{carbon,core}$/ I_{carbon}. Sufficient methane is injected to change f_{carbon}, but not to perturb other plasma conditions (n_e, T_e) significantly. To date, we have measured PF in only one experimental condition: ELMy H-mode with $n_e \sim 6 \times 10^{19}$ m^{-3}, finding PF ~ 20 ms. We use the measured main-wall carbon influx, Γ_{mw}, in order to assess the expected f_{carbon} caused by the intrinsic carbon erosion rate. Specifically,

$$f_{carbon} = \Gamma_{mw} \bullet PF \bullet A_{MW} / (V \bullet n_e), \tag{1}$$

where A_{MW} (m^2) is the area of the main wall, V (~ 20 m^3) is the volume of the DIII-D plasma. The main-wall carbon flux is determined from spectroscopy of low charge-states of carbon (typically C^{+1} from the outer midplane measured with the XUV survey spectrometer).

The second method to estimate f_{carbon} from main-wall sources uses the measured ionization rate of C^{+2} inside the LCFS (**Fig. 12**). This is obtained from the CIII (450 nm) tangential array at the outer midplane. Local emission is converted to local ionization rate, $S_{ion}(C^{+2})$, using calculated ionizations per photon (S/XB) ratios for the transition and measured plasma parameters. The core impurity level is then estimated by integrating the C^{+2} ionization rate inside the LCFS, namely:

$$f_{carbon} = (\int_{r<LCFS} S_{ion}(C^{+2}) \, dr) \bullet \tau_e \bullet A_{MW} / (V \bullet n_e), \tag{2}$$

where we estimate particle confinement time as being the energy confinement time (τ_e). C^{+2} is an ideal charge-state for this method: it is a sufficiently low ionization state that it
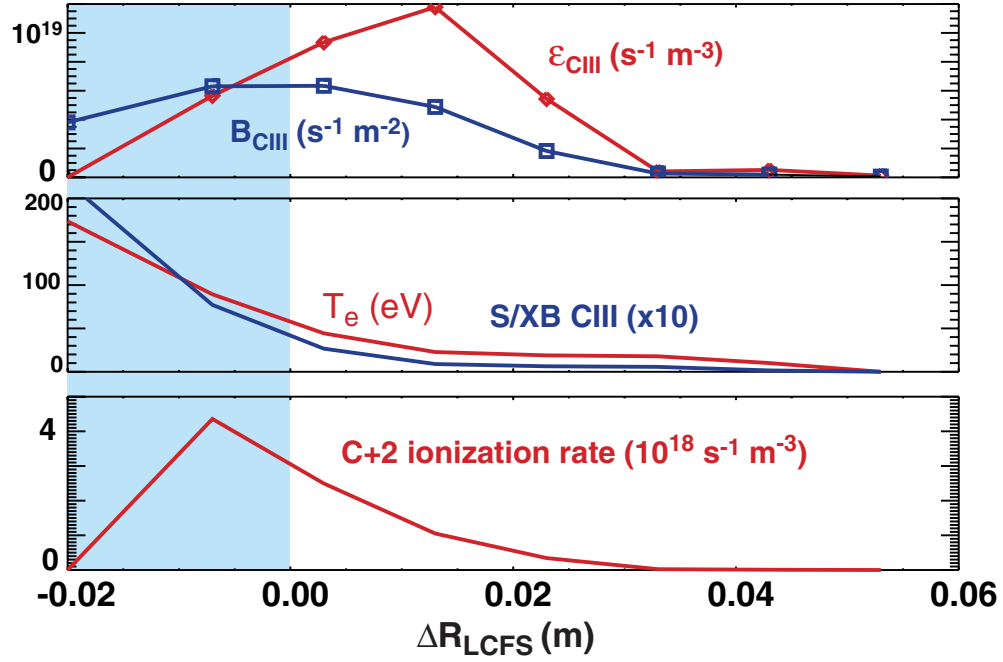
Fig. 12
Example of C^{+2} ionization profile measurements at outer midplane using tangential viewing array (Top) Brightness and emission profiles for CIII 465 nm emission. (Middle) Measured temperature profile and corresponding local ionizations per photon ratio S/XB for the transition (Bottom) Radial profile of C^{+2} ionization rate.

must arise from a SOL source, yet it is somewhat spatially dispersed by the SOL transport, thus mitigating the non-axisymmetries associated with the actual erosion source at the outer midplane.

The magnitude and penetration capability of main-wall sources is sufficient to explain core plasma impurity level in various confinement regimes and densities. In low density L-mode the C^{+2} ionization method accounts for f_{carbon} (**Fig. 13**). The C^{+2} ionization method also estimates the correct magnitude of f_{carbon} over a wide range of densities in H-mode (**Fig. 14**), from low recycling QDB discharge to fully detached ELMy H-mode. The penetrations factor method also estimates the correct magnitude of f_{carbon} at the density where PF has been measured ($\sim 6 \times 10^{19}$ m^{-3}). As can be seen in **Fig. 14**, f_{carbon} falls significantly away from the measured value at densities lower that this value, and increases sharply for higher densities. This implies that as expected the PF (or alternatively, impurity confinement time) is ihigher in the QDB case and degraded in the fully detached H-mode case. In another sense the SOL screening is improving with increasing density.

With convincing empirical evidence that the main-wall is the important location of erosion for controlling core impurity levels, it is desirable to ascertain the reason for the erosion at the main-wall surfaces. Namely, is the erosion caused solely by charge-exchange neutrals bombarding the wall (which would be controlled by leakage of neutrals from the divertor) or is it due to plasma flux to the main-wall surfaces? We note that if the latter is true, then both mechanisms will actually cause erosion due to the local SOL recycling caused by the plasma contact. Therefore, this question is best answered by assessing the magnitude of plasma contact with the main-wall surfaces. In particular we exploit the non-linear sensitivity (quadratic or more) of the edge plasma recycling to line-averaged density.

We use three methods to assess the flux to main-wall erosion surfaces: probes at main-wall surfaces, D_α recycling light and SOL plasma profiles. Recycling flux is estimated from measured D_α brightness using the well-known ionizations per photon method. For
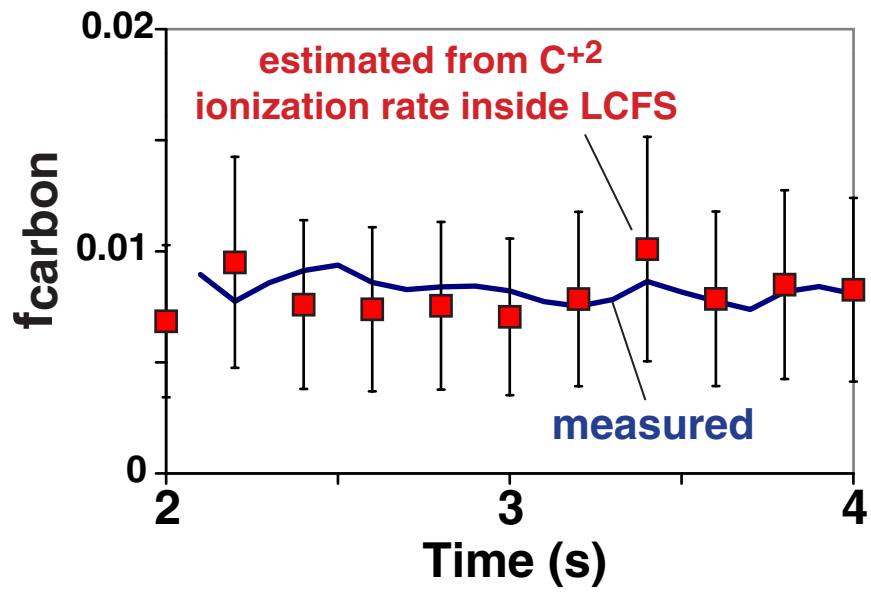
Time trace of measured core carbon fraction, f_{carbon}, compared to f_{carbon} expected from midplane C^{+2} ionization source in L-mode plasma: $P=1.8$ MW, $n_e = 2.25 \times 10^{19}$ m^{-3}.
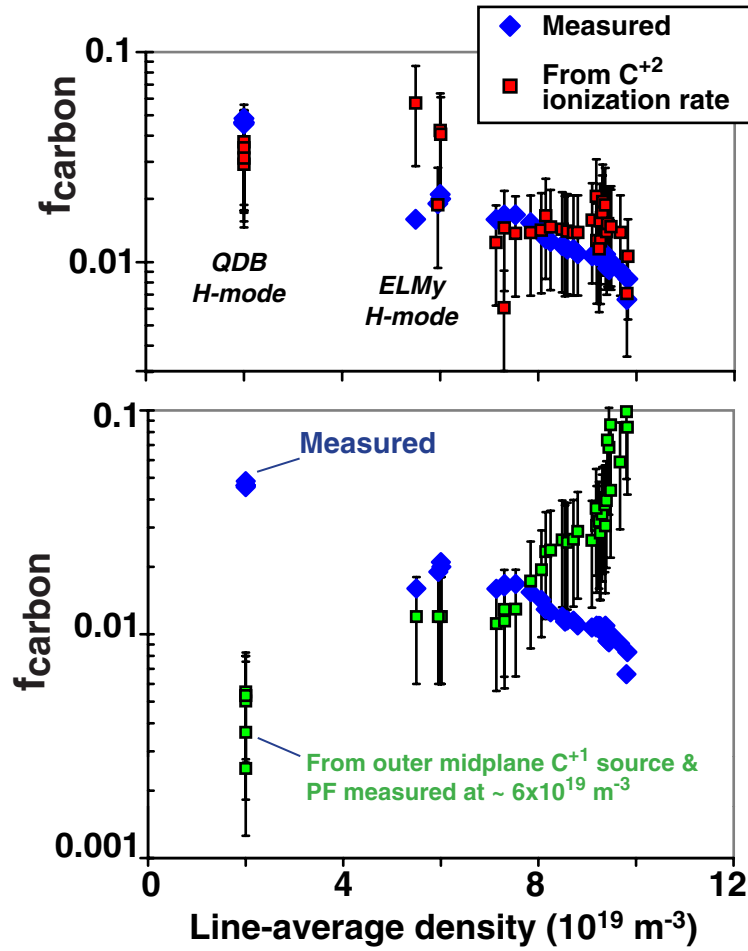
Fig. 14
Measured and expected core carbon fraction versus line averaged density. Expected f_{carbon} from: (Top) Midplane C^{+2} ionization source (Bottom) Penetration factor measured at $n_e \sim 6\times10^{19}$ m^{-3} combined with measured outer midplane C^{+1} erosion source from XUV spectroscopy. ELMy H-mode and non-ELMing, quiescent double-barrier (QDB) H-modes as noted.

the SOL plasma profile method, we integrate the expected parallel losses to axisymmetric limiting surfaces in the SOL in order to ascertain cross-field flux, Γ_{perp}, across the limiter flux surface. Specifically,

$$\Gamma_{perp} \sim 2\, n_e\, c_s\, \lambda_r\, L_{par}, \tag{3}$$

where c_s is sound speed, λ_r is the fitted radial e-folding length of $n_e c_s$ behind the limiter shadow, L_{par} is the parallel field line length between the limiting surface. For DIII-D we use the upper baffle knee limiter, the inner wall and the outer lower baffle structure as possible limiting surfaces. SOL profiles are measured with either Thomson scattering or the midplane scanning probe. We have verified the expected $n_e c_s$ parallel flux to the limiting surface using the Langmuir probe in the upper baffle knee.

The magnitude and trends of plasma contact at main-wall surface is consistent with measured erosion and recycling. This is true even when gaps between the LCFS and main-wall surfaces are relatively large. See for example the lower panel of **Fig. 10**: the carbon source correlates to the directly measured plasma flux to the limiter at all gap distances. This is also true for the outer midplane in both L-mode and ELMy H-mode (**Fig. 9**). We also note that both chemical (B_{CD}) and physical sputtering ($T_e > 10$ eV) occur at the outer midplane (**Fig. 9**). Plasma flux, recycling and impurity source at the main-wall increase non-linearly with increasing density (i.e. $\Gamma \propto n_e^{2.5-5}$.). The magnitude and trends of main-wall plasma flux and main-wall recycling agree very well in both L-mode (**Fig. 15**) and in ELMy H-mode (**Fig. 16**). The spectroscopically measured erosion flux of carbon from the main-wall surfaces follows the trend of main-wall plasma flux with density and has the expected yield ~ 1-3%.

A consequence of the strong plasma flux to the wall versus density is that as the divertor detaches the main-wall becomes the dominant location of erosion and plasma-conducted heat flux. At detachment, the main-wall carbon source dominates over the divertor (**Fig. 17**). The cold divertor no longer sustains physical sputtering, while plasma flux and erosion at the main-wall continue to increase strongly with n_e. At detachment, plasma conducted heat to main-wall is significant (~15% P_{in}) as shown in **Fig. 18**. After detachment, the cold divertor ($T_e \sim 1$ eV) no longer sustains heat conduction to the divertor targets. In fact, main-wall plasma flux and the associated conducted heat are needed to
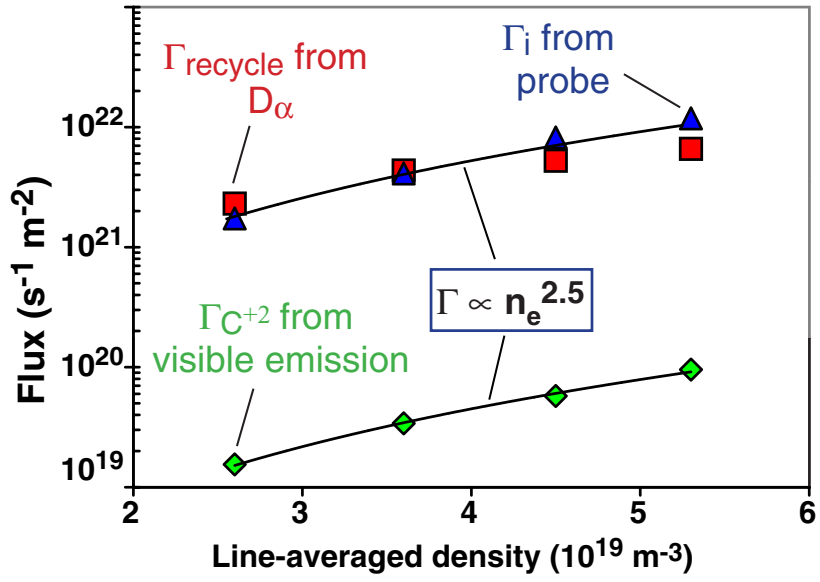
Fig. 15
Measured plasma flux (probe), recycling flux from D_α , and carbon flux (C^{+2}) at the baffle knee/limiter during density scan. Discharge: L-mode, P ~ 1.8 MW.
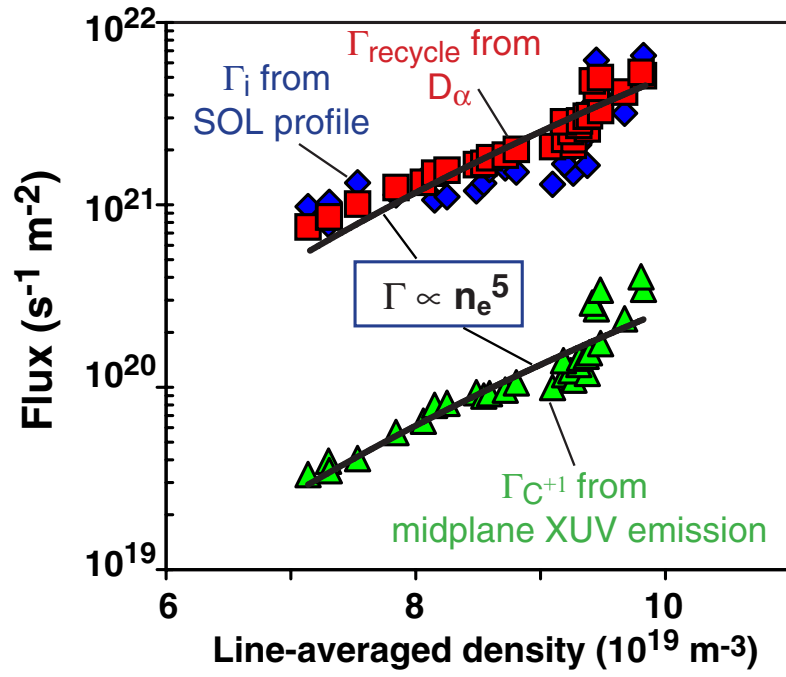
Fig. 16
Measured plasma flux (from SOL profiles), recycling flux from D_α, and carbon flux (C^{+1}) from the outer midplane limiter during density scan. Discharge: ELMy H-mode, $P \sim 7$ MW.
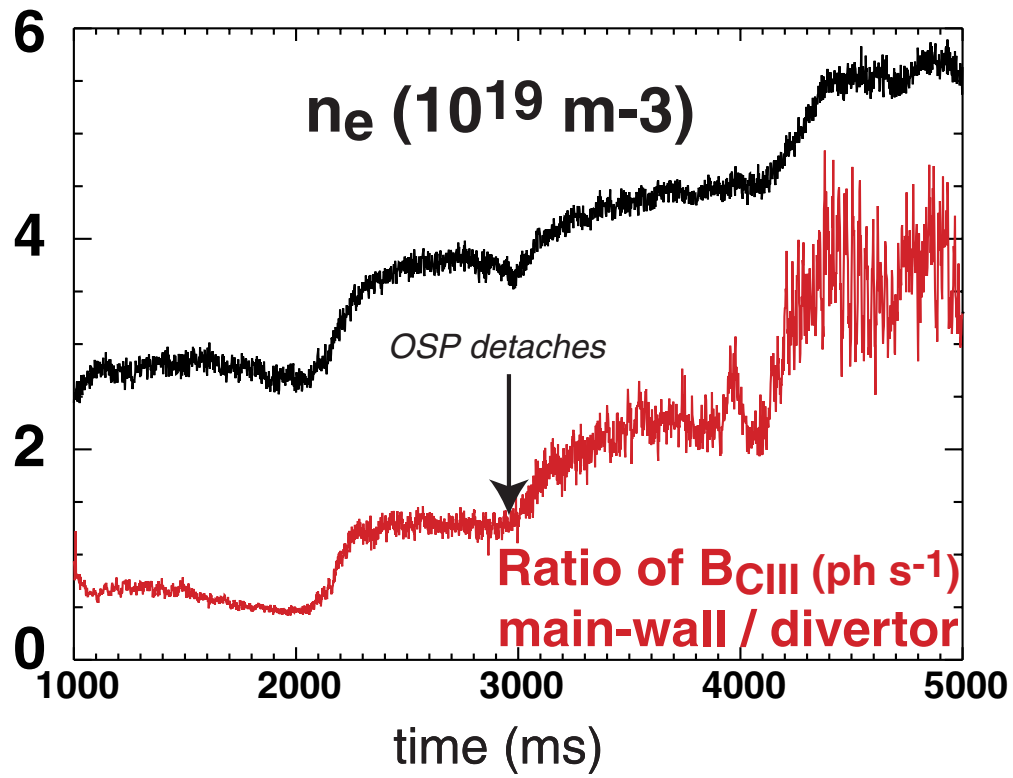
Fig. 17
Ratio of CIII main-wall to divertor photon emission rates (photons s^{-1}) during density scan in L-mode discharge (P~1.8 MW).
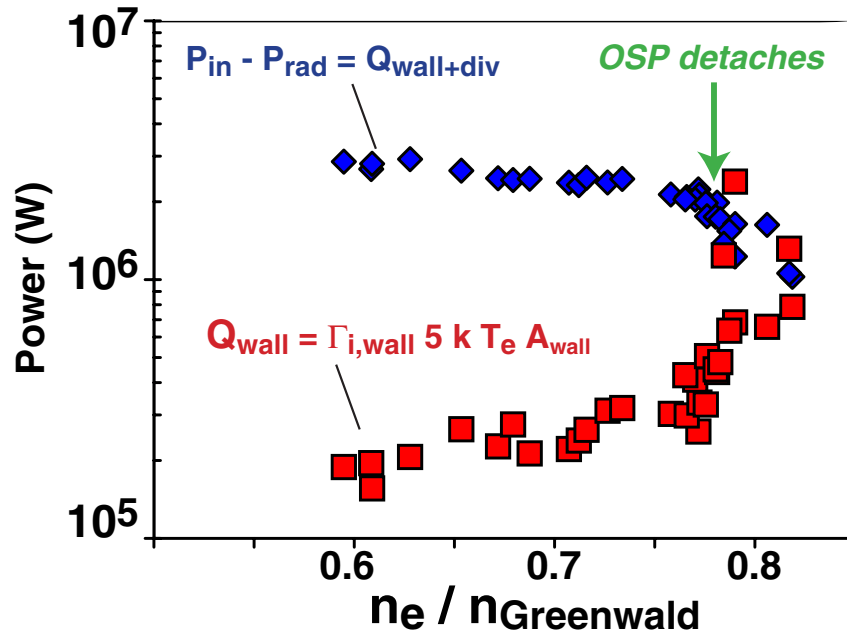
Fig. 18
Power balance in ELMy H-mode (P~7 MW) discharge with density scan to detachment.
Total plasma-conducted heat flux to wall, Q_{wall}, cross-field plasma-conducted heat to the
main-wall, Q_{perp} based on Γ_{perp} are shown.

satisfy global power balance. A final confirmation of the dominance of main-wall erosion in detachment is the observation that the entire divertor is a region of net carbon deposition for detached plasmas.

4. Discussion on implications of main-wall erosion

Empirical evidence strongly indicates that plasma flux to the main-wall surfaces is the erosion mechanism controlling core impurity levels. Naturally the question arises on the nature of the SOL transport that gives rise to this observation.

We use the assumption of local particle balance (i.e. local recycle flux = local plasma flux) to assess SOL transport in L-mode and H-mode versus increasing density (**Fig. 19**). SOL plasmas profiles are measured with Thomson scattering. Local ionization rates are measured with the tangential midplane D_α array (**Fig. 8**). Cross-field plasma transport is obtained by radially integrating ionization source and the effective cross-field convective velocity is obtained from normalizing the density, $v_{eff} = \Gamma_{perp} / n_e$. As density increases the SOL density becomes essentially flat, extending out to limiter surfaces, while temperature remains relatively constant. This allows for the large increases in carbon sputtering versus density as shown in the previous section. In a sense, the empirical observations on main-wall erosion provide a useful tool in assessing the magnitude of SOL cross-field transport.

It is worthwhile to note that v_{eff} in the far SOL is approximately constant versus density and is only changed by switching confinement regimes. This implies that the broad SOL densities are a product of the convective (and presumably turbulent) nature of the SOL transport. Also, the magnitude of v_{eff} (10-50 m/s) is sufficiently high that one expects radial particle transport to compete effectively against parallel losses to the divertor.

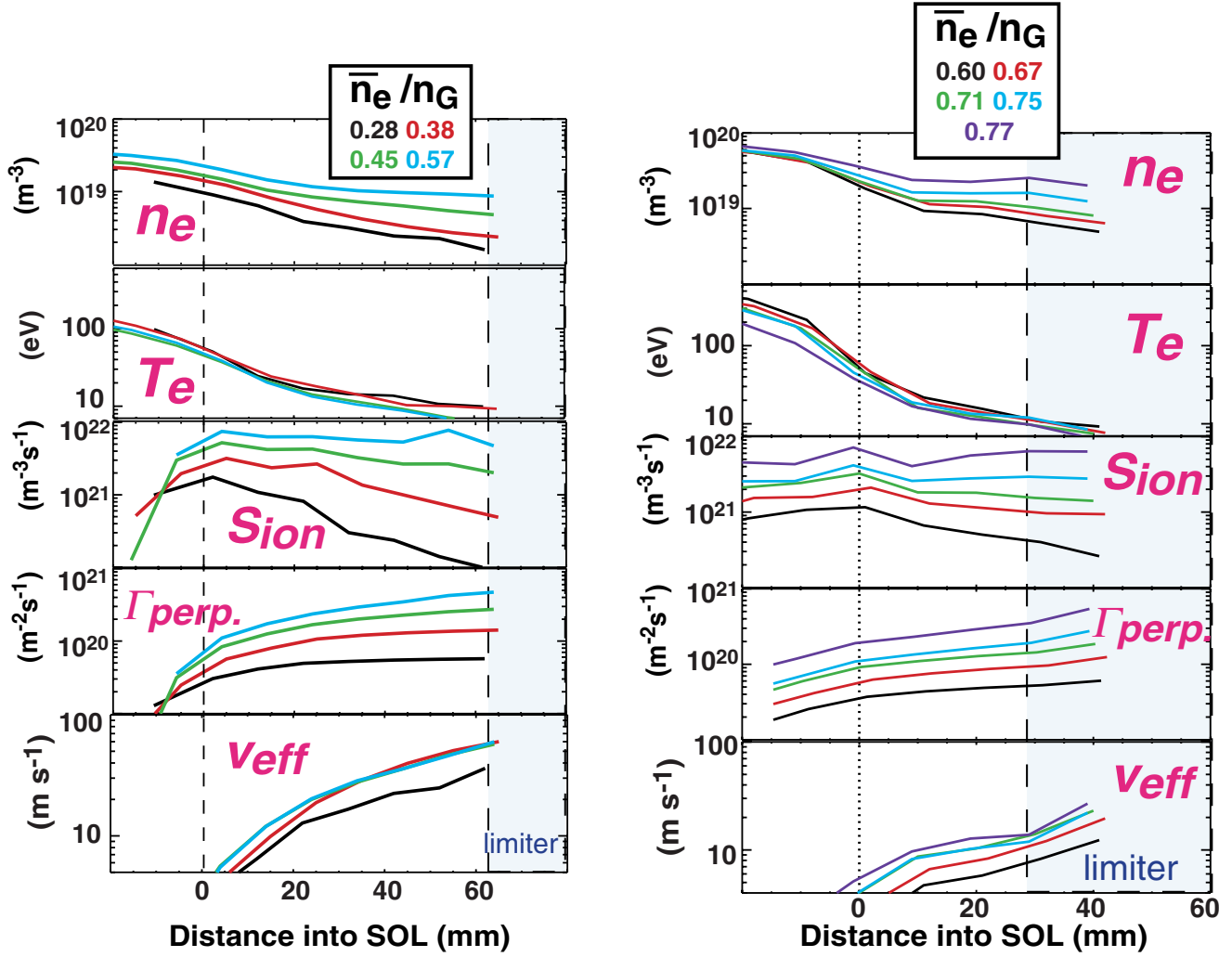The implications of main-wall erosion caused by plasma contact ripple through edge issues in current devices.

Fig. 19
SOL transport analysis based on local particle balance for (left) L-mode (P~1.8 MW) and (right) ELMy H-mode (P~7 MW) discharges with density scans. Density and temperature from Thomson scattering. Midplane ionization rates from inversion of tangential D_α. Perpendicular plasma flux, Γ_{perp}, from radially integrating local ionization source. Effective local convective cross-field velocity, v_{eff}, from Γ_{perp}/n_e.

- High f_{carbon} in many high performance discharges, clearly a concern in the extrapolation of such operational modes to burning plasma experiments.
- Global erosion/redeposition patterns that is inconsistent with divertor sources alone. This includes the JET *beryllium* divertor operation that collected *carbon* (the main-wall limiter material) deposits at the inner divertor and the observation of divertor net deposition in DIII-D during detachment.
- Tritium retention in the JET divertor that must seemingly be explained by substantial non-divertor sources.
- Main-wall impurity source suggests strongly the possibility that the main-wall recycling also controls refueling. This links also then to issue of pedestal physics and core plasma performance?

5. Summary

The Poloidal divertor configuration has better impurity control than limiter configuration. Evidence indicates the divertor works so well at screening impurities that the main-wall surfaces, not divertor targets, are the controlling location of impurities for core plasma contamination. Plasma flux to the main-wall drives erosion processes that leads to core impurity levels. In general, as density is increased through divertor detachment plasma flux to the main-wall increases dramatically, while physical erosion is eliminated in the divertor. The main-wall becomes then the dominant location of total erosion. A better understanding of the SOL transport processes that lead to main-wall erosion is needed.

References

[1] C.S. Pitcher, P.C Stangeby, Plasma Phys. Contr. Fusion **39** (1997) 779.

[2] M.E. Fenstermacher, et al. J. Nucl. Mater. **241-243** (1997) 667.

[3] D.G. Whyte, et al., Nucl. Fusion **38** (1998) 387.

[4] D.N. Hill et al. 20th EPS Conference on Controlled Fusion and Plasma Physics, Lisboa 1993, **Vol 2** (1993) II-643.

[5] D.G. Whyte, R.P. Doerner, Physica Scripta **T91** (2001) 7.

[6] H.Y. Guo, et al Nucl Fusion **40** (2000) 379.

[7] D.G; Whyte, et al. J. Nucl. Mater. **290-293** (2001) 356.

[8] J. W. Davis et al J. Nucl. Mater. . **290-293** (2001) 66.